

# Evolutionary algorithm-based PID controller tuning for nonlinear quarter-car electrohydraulic vehicle suspensions

Muhammed Dangor · Olurotimi A. Dahunsi · Jimoh O. Pedro · M. Montaz Ali

Received: 28 October 2013 / Accepted: 26 July 2014  
© Springer Science+Business Media Dordrecht 2014

**Abstract** The basic challenge associated with the design of vehicle suspension system is the attainment of an optimal trade-off between the various design objectives. This study presents the design of proportional-integral-derivative (PID) controller for a quarter-car active vehicle suspension system (AVSS) using evolutionary algorithms (EA) such as the particle swarm optimization (PSO), genetic algorithm (GA) and differential evolution (DE). Each of the EA-based PID controllers showed overall improvement in suspension travel, ride comfort, settling time and road holding from the manually tuned controller and the passive vehicle suspension system. These improvements were, however, achieved at the cost of increased actuator force,

power consumption and spool-valve displacement. DE-optimized PID control resulted in the best minimized suspension performance, followed by the GA and PSO, respectively. Frequency-domain analysis showed that all the signals were attenuated within the whole body vibration frequency range and the EA-optimized controllers had RMS frequency weighted body acceleration of the vehicle within allowable limits for vibration exposure. Robustness analysis of the DE-optimized PID-controlled AVSS to model uncertainties is carried out in the form of variation in vehicle sprung mass loading, tyre stiffness and speed.

**Keywords** Force feedback · PID control · Active vehicle suspension system · Genetic algorithm · Particle swarm optimization · Differential evolution

---

M. Dangor · O. A. Dahunsi · J. O. Pedro (✉)  
School of Mechanical, Industrial and Aeronautical Engineering, University of the Witwatersrand, 1 Jan Smut Avenue, Private Bag 03, Johannesburg WITS 2050, South Africa  
e-mail: Jimoh.Pedro@wits.ac.za;  
jimoh.olarewaju.pedro@gmail.com

M. Dangor  
e-mail: mdangor98@gmail.com

O. A. Dahunsi  
e-mail: tundedahunsi@gmail.com

M. M. Ali  
Faculty of Science, and TCSE, Faculty of Engineering and Built Environment, School of Computational and Applied Mathematics, University of the Witwatersrand, 1 Jan Smut Avenue, Private Bag 03, Johannesburg WITS 2050, South Africa  
e-mail: Montaz.Ali@wits.ac.za

## 1 Introduction

A vehicle suspension system is made up of springs, dampers and linkages connected together in such a way that it supports the weight of the vehicle. It also serves to isolate the vehicle from road disturbances propagated via its wheels, enhances road holding and handling capabilities, and maintains suspension travel within the physical constraints allowed for in the rattle space [1–3].

Vehicle suspension systems are available in three configurations, namely: passive vehicle suspension system (PVSS), semi-active vehicle suspension system

(SAVSS) and active vehicle suspension system (AVSS). While the PVSS remains the most popular based on its simplicity and low-cost, its fixed design parameters do not allow for flexibility and adaptive performance. Controllable dampers makes SAVSS to perform better than the PVSS, but the AVSS holds better prospect. AVSS responds dynamically to road disturbance inputs. It induces relative motion between the body and the wheel through the actuator force it generates.

The fundamental challenge in AVSS design is determining an optimal *trade-off* between these conflicting design objectives. This must be done in such a way that the overall performance is enhanced in spite of inherent nonlinearities and uncertainties in the system.

Evidence in the literature shows the superior performance of the AVSS in terms of these design objectives, but the choice of appropriate control method is vital [2–5]. Recent advances in control engineering, sensors, actuators and digital electronic systems today have enhanced the capacity for more computationally demanding control schemes on AVSS. However, setbacks due to cost and hardware constraints still remain [6, 7].

Large proportion of the control techniques employed in AVSS design are linear control schemes [8–12]. Linear optimal control schemes are attractive because they are stable and robust, but are limited in the face of complex nonlinear AVSS behaviour associated with hydraulic or pneumatic actuator dynamics. Moreover, most AVSS applications of linear optimal control schemes presume time-invariant situation [13–16].

Examples of nonlinear control schemes that have been applied in AVSS designs are: sliding mode, backstepping and feedback linearization (FBL). Backstepping control method is increasingly being employed in the literature to solve the AVSS problem because of its adaptive control strengths. Its setback is, however, repeated differentiation of the system nonlinear function which leads to an increase in complexity of the nonlinear functions [17–19]. Exact FBL is not always possible because full knowledge of the nonlinear system model is always required. Input–output FBL, however, requires an elaborate internal stability analysis.

While sliding mode control holds good prospect, being adaptive, the presence of *chattering* is a setback that could degrade the system performance by

exciting unmodelled high-frequency dynamics due to the switching control signal [15, 20]. Its successful application is dependent on availability of good system dynamic model since it uses the function approximation technique [21, 22]. It is also susceptible to measurement noise and requires large control signals [20].

PID control remains the most popular industrial control structure because of its simplicity. Transient and steady-state characteristics such as overshoot, rise-time and settling-time are improved by simply adjusting the controller gains [23–25]. PID applications in AVSS design have remained limited except for the purpose of performance benchmarking because of robustness limitations that is attributed to ineffective tuning [26]. However, PID control holds great prospect when combined with an appropriate intelligent control technique, especially for nonlinear systems [27, 28].

Documented results have shown that large percentage of industrial PID control application are either manually -tuned, poorly tuned or used based on its default settings. Meanwhile, the best benefit of PID control applications can only be assessed with appropriate tuning [24, 25]. Zeigler–Nichols and Cohen tuning methods [25] have been successfully employed for decades, but they have a tendency to increase oscillation of the signals and become more cumbersome to apply in multi-loop cases like the one under consideration.

These shortcomings in PID control have been tackled through its combination with fuzzy control in several documented works [29–33]. Improved performance was recorded because of fuzzy control's strength as a nonlinear controller that is implemented where model information available is inadequate. However, obtaining the fuzzy control rules is time consuming and not straight forward; thereby requiring EA like PSO or GA for tuning purposes [8, 31–34]. This increases computational challenges in the system, thus prompting the use of EA in optimizing the PID gains directly.

EA are global optimization search techniques whose operations mimic biological or natural processes. They provide quick means to attain the expected optimal specifications if suitable initial conditions are provided [6, 31, 35, 36]. GA, PSO and DE are heuristic, population set-based direct search global optimization algorithms with wide applications. They generate newer and improved solutions through processes similar to biological evolution processes [14, 37–39]. These

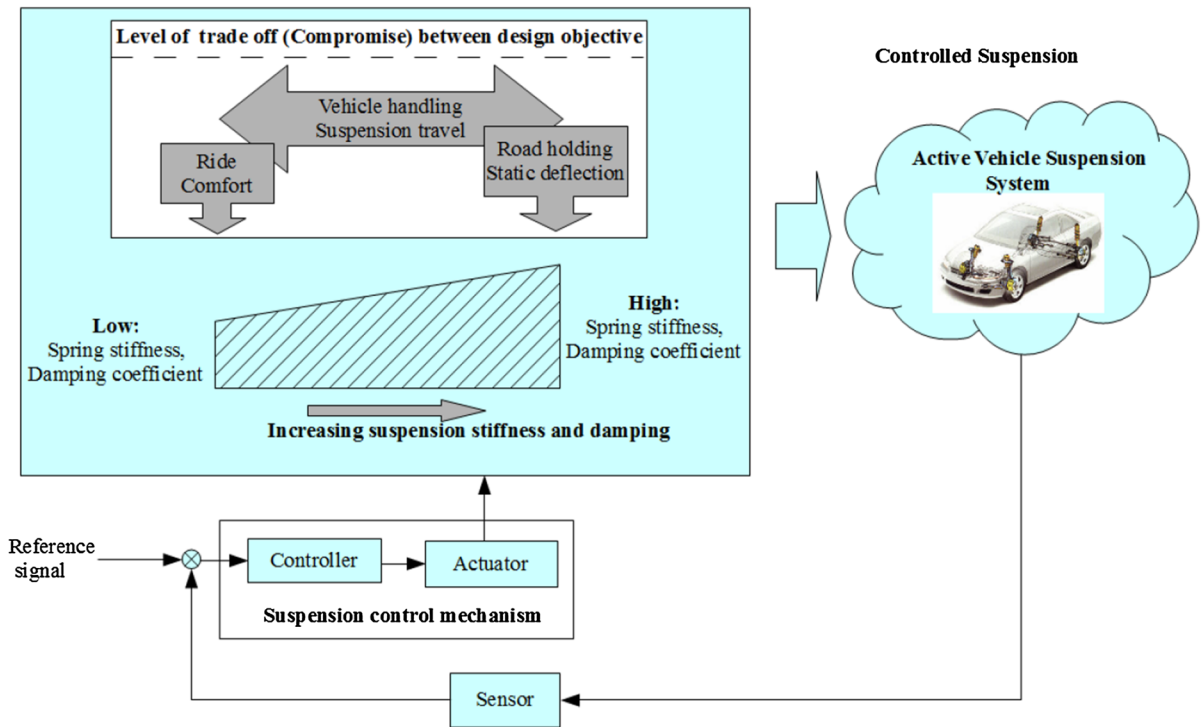


Fig. 1 AVSS feedback control loop

characteristics make EA to be robust and flexible, but care must be taken in the selection of the particular EA for a control problem. Factors to consider must include computational efficiency and real-time implementation [36,39].

PSO is inspired by the migration of swarms and bears some similarities with GA, which is inspired by the biological reproductive process; for example, it also generates improved results after each generation. Its result may, however, show a weak progression in the initial stages and take significant amount of time converging [40–42]. Although DE has been shown to be very efficient in some applications, it tends to be computationally expensive with respect to the number of objective function evaluations [39,43,44].

The rest of the paper is structured as follows. The next section presents a brief description of the physical model, mathematical model and road disturbance input models. The third section highlights the system specifications and evaluation criteria. The fourth section presents the controller design and optimization methods. Discussion of results is presented in the fifth section and this is followed by the concluding remarks in the last section.

## 2 System modelling

Figure 1 presents the generic AVSS feedback control loop. The system consists of a controller issuing the command input to the actuator to generate a manipulating signal. Better command input signal is sent because the controller output is optimized by the use of EA.

AVSS responds dynamically to road disturbance inputs by inducing relative motion between the body and the wheel through the force generated by the servo-hydraulic actuator. Obtaining the appropriate control voltage for the actuator includes optimal trade-off between the design objectives in the presence of road disturbance inputs. The success of this process yields a suspension system that is adaptive to the road disturbance and other operating conditions.

### 2.1 Mathematical model

The physical system used for this investigation is a 2DOF, quarter-car suspension model shown in Figure 2. This model readily captures the body heave and wheel hop vibration mode. The sprung mass (chassis) is represented by  $m_s$ , unsprung mass (wheel)  $m_u$ .  $k_s$

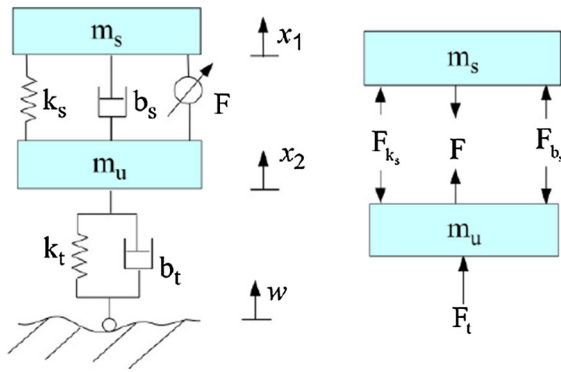


Fig. 2 Simplified quarter-car model

and  $k_t$  are the suspension and wheel stiffnesses, respectively.  $b_s$  is the damping coefficient of the suspension system,  $b_t$  is the damping coefficient of the tyre (which in this case is taken to be zero),  $F$  is the actuator force,  $x_1$  and  $x_2$  are the vertical displacements of the chassis and wheel, respectively, while  $w$  is the road disturbance input. The controlled variable is represented by the suspension travel ( $x_1 - x_2$ ),  $\ddot{x}_1$  is the body-heave acceleration which characterizes the ride comfort and  $(x_2 - w)$  represents the wheel deflection which characterizes road holding quality.

Application of Newton’s law to the quarter-car model shown in Fig. 2 yields the following nonlinear governing equations [1, 45]:

$$\begin{aligned}
 F_{m_s} &= m_s \ddot{x}_1 \\
 F_{m_u} &= m_u \ddot{x}_2 \\
 F_{k_s} &= k_s^l (x_2 - x_1) + k_s^{nl} (x_2 - x_1)^3 \\
 F_{k_t} &= k_t (x_2 - w) \\
 F_{b_t} &= b_t (\dot{x}_2 - \dot{w}) \\
 F_t &= F_{k_t} + F_{b_t} \\
 F_{b_s} &= b_s^l (\dot{x}_2 - \dot{x}_1) - b_s^{sym} |\dot{x}_2 - \dot{x}_1| \\
 &\quad + b_s^{nl} \sqrt{|\dot{x}_2 - \dot{x}_1|} \operatorname{sgn}(\dot{x}_2 - \dot{x}_1) \\
 F &= A x_p
 \end{aligned}$$

therefore:

$$\begin{aligned}
 F_{m_s} &= F_{k_s} + F_{b_s} - F \\
 m_s \ddot{x}_1 &= k_s^l (x_2 - x_1) + k_s^{nl} (x_2 - x_1)^3 + b_s^l (\dot{x}_2 - \dot{x}_1) \\
 &\quad - b_s^{sym} |\dot{x}_2 - \dot{x}_1| + b_s^{nl} \sqrt{|\dot{x}_2 - \dot{x}_1|} \operatorname{sgn}(\dot{x}_2 - \dot{x}_1) \\
 &\quad - A x_p
 \end{aligned} \tag{1}$$

and

$$\begin{aligned}
 F_{m_u} &= -F_{k_s} - F_{b_s} + F_{k_t} + F_{b_t} + F \\
 m_u \ddot{x}_2 &= -k_s^l (x_2 - x_1) - k_s^{nl} (x_2 - x_1)^3 - b_s^l (\dot{x}_2 - \dot{x}_1) \\
 &\quad + b_s^{sym} |\dot{x}_2 - \dot{x}_1| - b_s^{nl} \sqrt{|\dot{x}_2 - \dot{x}_1|} \operatorname{sgn}(\dot{x}_2 - \dot{x}_1) \\
 &\quad + k_t (x_2 - w) + b_t (\dot{x}_2 - \dot{w}) + A x_p
 \end{aligned} \tag{2}$$

also

$$\begin{aligned}
 \frac{V_t}{4\beta_e} \dot{x}_p &= Q - C_{lp} x_p - A (\dot{x}_1 - \dot{x}_2) \\
 \dot{x}_p &= \alpha Q - \beta x_p - \alpha A (\dot{x}_1 - \dot{x}_2)
 \end{aligned} \tag{3}$$

where:

$$\alpha = \frac{4\beta_e}{V_t}, \quad \beta = \alpha C_{lp} \quad \text{and}$$

$$Q = \operatorname{sgn}[P_s - \operatorname{sgn}(x_v) x_p] C_d S x_v \sqrt{\frac{1}{\rho} |P_s - \operatorname{sgn}(x_v) x_p|}$$

The suspension spring and damping forces have linear and nonlinear components. Spring constant,  $k_s^l$ , and damping coefficient,  $b_s^l$ , affect the spring force and damping force in linear manner.  $b_s^{sym}$  contributes an asymmetric characteristics to the overall behaviour of the damper.  $k_s^{nl}$  and  $b_s^{nl}$  are responsible for the nonlinear components of the spring and damper forces, respectively.  $P_s$  is the supply pressure into the hydraulic cylinder,  $A$  is the area of the piston,  $V_t$  is the total actuator volume,  $\beta_e$  is the effective bulk modulus of the system,  $C_{lp}$  is the total leakage coefficient of the piston,  $C_d$  is the discharge coefficient,  $S$  is the spool-valve area gradient and  $\rho$  is the hydraulic fluid density.

The electrohydraulic system is modelled as a first-order dynamic system with a time constant  $\tau$ .

$$\dot{x}_v = \frac{1}{\tau} (-x_v + K_v u) \tag{4}$$

where  $K_v$  is the servo-valve gain. Supply voltage of range  $\pm 10V$  is supplied to the servo-valve as control input to limit the suspension travel to  $\pm 10cm$  [15].

Using the state-space representation, the system governing equations can be presented as:

$$\dot{\mathbf{x}} = \mathbf{f}(\mathbf{x}) + \mathbf{g}(\mathbf{x})u + \mathbf{p}(\mathbf{w}) \tag{5}$$

$$y = h(\mathbf{x}) = x_2 - x_1 \tag{6}$$

where the state vector  $\mathbf{x} = [x_1 \ x_2 \ x_3 \ x_4 \ x_5 \ x_6]^T$ , the output variable  $y = x_2 - x_1$ , and the control input  $\mathbf{u}$ . The system matrices  $\mathbf{f}$  and  $\mathbf{g}$  are:

$$\mathbf{f}(\mathbf{x}) = [f_1(x) \ f_2(x) \ f_3(x) \ f_4(x) \ f_5(x) \ f_6(x)]^T, \tag{7}$$

where

$$f_1(x) = x_3 \tag{8}$$

$$f_2(x) = x_4 \tag{9}$$

$$f_3(x) = \frac{1}{m_s} \left[ k_s^l(x_2 - x_1) + k_s^{nl}(x_2 - x_1)^3 + b_s^l(x_4 - x_3) - b_s^{sym}|x_4 - x_3| + b_s^{nl}\sqrt{|x_4 - x_3|}sgn(x_4 - x_3) - Ax_5 \right] \tag{10}$$

$$f_4(x) = \frac{1}{m_u} \left[ -k_s^l(x_2 - x_1) - k_s^{nl}(x_2 - x_1)^3 - b_s^l(x_4 - x_3) + b_s^{sym}|x_4 - x_3| - b_s^{nl}\sqrt{|x_4 - x_3|}sgn(x_4 - x_3) + k_t x_2 + b_t \dot{x}_2 + Ax_5 \right] \tag{11}$$

$$f_5(x) = \gamma \Phi x_6 - \beta x_5 - \alpha A(x_3 - x_4) \tag{12}$$

$$f_6(x) = \frac{-x_6}{\tau} \tag{13}$$

$$\mathbf{g}(\mathbf{x}) = [0 \ 0 \ 0 \ 0 \ 0 \ \frac{1}{\tau}]^T \tag{14}$$

$$\mathbf{p}(\mathbf{w}) = [0 \ 0 \ 0 \ -(\frac{k_t}{m_u} w + \frac{b_t}{m_u} \dot{w}) \ 0 \ 0]^T \tag{15}$$

where  $x_3$  and  $x_4$  are vertical velocities of the sprung and unsprung masses, respectively,  $x_5$  is the pressure drop across the piston,  $x_6$  is the servo-valve displacement and  $\Phi$  is the hydraulic load flow.

Figure 3 represents the hydraulic actuator mounted in between the sprung and unsprung masses.  $Q_u$  and  $Q_l$  are the hydraulic fluid flow rates into the upper and lower chambers of the cylinder, respectively.  $P_r$  is the return pressure from the hydraulic cylinder,  $P_u$  and  $P_l$  are the oil pressures in the upper and lower portion of the cylinder.

The performance of the suspension system is evaluated at the vehicle travelling speed of 40 km/h in the presence of a road disturbance input with sinusoidal profile, half-wavelength of 5 m and amplitude of 11 cm. The profile of the bump is modelled by Eq. (16) and illustrated in Fig. 4.

$$w(t) = \begin{cases} \frac{a}{2}(1 - \cos\frac{2\pi Vt}{\lambda}) & 0.45 \leq t \leq 0.9 \\ 0 & \text{otherwise} \end{cases} \tag{16}$$

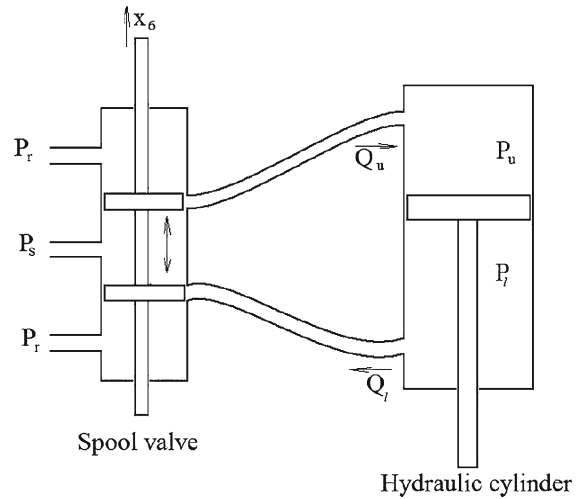


Fig. 3 Schematic of the double-acting hydraulic strut

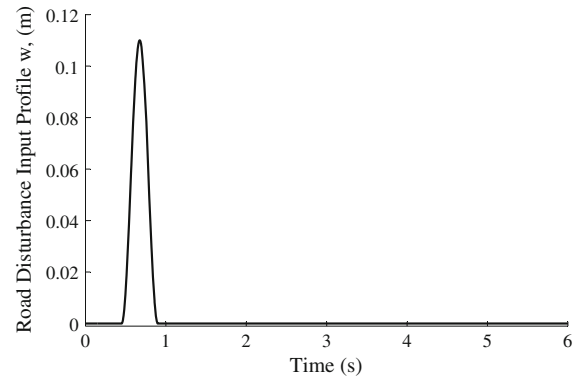


Fig. 4 Road disturbance input profile

where  $a$  is the bump height,  $V$  is the vehicle’s velocity in straight line and  $\lambda$  is the half wavelength of the sinusoidal road undulation. The values for the system parameters are provided in Table 1.

### 3 System performance specification and evaluation

#### 3.1 Performance specifications

The following characteristics are required of the AVSS controller in a bid to meet the set performance objectives:

1. **Nominal stability:** The closed loops should be nominally stable. Stability of the actuator dynamics is enhanced through an inner loop force feedback. This should improve the overall system stability.

**Table 1** Parameters of the quarter-car model [45]

Parameters	Value	Parameters	Value
Sprung mass, $m_s$	290kg	Suspension stiffness (linear), $k_s^l$	$2.35 \times 10^4 \text{N/m}$
Unsprung mass, $m_u$	40kg	Suspension stiffness (nonlinear), $k_s^{nl}$	$2.35 \times 10^6 \text{N/m}$
Tyre stiffness, $k_t$	$1.9 \times 10^5 \text{N/m}$	Suspension damping (linear) ( $b_s^l$ )	700 N/m
Bump height, $a$	0.11 m	Suspension damping (nonlinear) ( $b_s^{nl}$ )	400 Ns/m
Piston area, $A$	$3.35 \times 10^{-4} \text{m}^2$	Suspension damping (asymmetrical), $b_s^{sym}$	400 Ns/m
Actuator time constant, $\tau$	$3.33 \times 10^{-2} \text{s}$	Actuator parameter ( $\alpha$ )	$4.515 \times 10^{13}$
Supply pressure ( $P_s$ )	10, 342, 500 Pa	Actuator parameter ( $\beta$ )	1
Vehicle speed ( $V$ )	40 km/h	Actuator parameter ( $\gamma$ )	$1.545 \times 10^9$
Disturbance half wavelength ( $\lambda$ )	5 m		
Servo-valve gain ( $K_v$ )	0.001 m/V		

- Disturbance rejection:** The designed controller should be able to attenuate low-frequency disturbance inputs.
- Good command following:** The suspension travel response of the AVSS is examined in the presence of the deterministic road input shown in Fig. 4. The controller should be able to keep the steady-state error as close as possible to zero.
- Suspension travel:** is constrained to physical limits to avoid damages due to topping and bottoming. Thus it is not to exceed  $\pm 0.1\text{m}$  [15].
- The **control voltage** is also limited to  $\pm 10\text{V}$ .
- The maximum **actuator force** must be less than the static weight of the vehicle, that is  $F_{a_{max}} < m_s g$ .
- For good **road holding** the dynamic load that is transmitted through the road should not be larger than the static weight of the vehicle.
- Ride comfort:** This is quantified using the vehicle body acceleration in the vertical direction. The vertical acceleration of the vehicle body needs to be minimal for good ride comfort, especially within the low-frequency band of 0.1 to 10Hz. The peak sprung mass acceleration:  $\ddot{x}_1 < 4.5\text{m/s}^2$  [46–49].

The objective function employed in the optimization algorithms is presented in Eq. (17). It is designed to minimize the suspension travel,  $y$ , actuator force,  $F_a$ , sprung mass acceleration,  $\ddot{x}_1$ , actuator spool-valve displacement,  $x_6$ , control voltage,  $u$ , and wheel deflection,  $(x_2 - w)$ . This way, ride comfort and road holding is

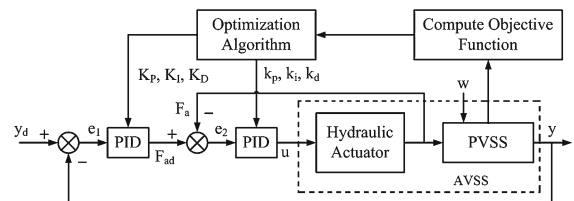


**Fig. 5** Control architecture

improved while control voltage and actuator force is kept as small as possible.

$$J = \frac{1}{T} \int_0^T \left[ \left( \frac{y}{y_{max}} \right)^2 + \left( \frac{F_a}{F_{a_{max}}} \right)^2 + \left( \frac{\ddot{x}_1}{\ddot{x}_{1_{max}}} \right)^2 + \left( \frac{x_6}{x_{6_{max}}} \right)^2 + \left( \frac{u}{u_{max}} \right)^2 + \left( \frac{(x_2 - w)}{(x_2 - w)_{max}} \right)^2 \right] dt \tag{17}$$

### 4 Controller design and implementation

Figure 5 shows the controller architecture for the multi-loop AVSS. The inner loop is used for force feedback control while the outer loop is used for the suspension travel feedback control. The outer loop is also used for disturbance rejection control (i.e. it attenuates the unwanted disturbances from the uneven road surface).  $y_d$  is the desired suspension travel,  $e_1$  and  $e_2$  are error signals that will be minimized in the outer and inner

control loops, respectively,  $F_a$  is the actuator force that will be regulated in the inner control loop with  $F_{ad}$  being its respective setpoint,  $y$  is the actual suspension travel that will be manipulated through the outer control loop, and  $u$  is the control input signal that is passed into the AVSS by the controller.

The objective function used is based on the various AVSS design specifications and goals, and it employs a number of component functions to enhance the optimization algorithms in selecting optimal gains for the PID loops. The performance of the PID loops are based on the minimization of mean squared error (MSE) of the component functions.

#### 4.1 Controller structure

The PID controller is defined by [26]:

$$e_1(t) = y_d - y \tag{18}$$

$$F_{ad}(t) = K_P e_1(t) + K_I \int e_1(t)dt + K_D \frac{de_1(t)}{dt} \tag{19}$$

$$e_2(t) = F_{ad}(t) - F_a(t) \tag{20}$$

$$u(t) = k_p e_2(t) + k_i \int e_2(t)dt + k_d \frac{de_2(t)}{dt} \tag{21}$$

where  $k_p$  and  $K_P$  are the proportional gains of the inner and outer loops, respectively,  $k_i$  and  $K_I$  are the corresponding integral gains of the controllers, and  $k_d$  and  $K_D$  are the derivative gains of the respective control loops. For the system to be set up as a regulation control problem, the reference signal  $y_d$  was set to zero. It is therefore desired that a control law  $F_{ad}(t)$  be designed such that  $e_1(t) \rightarrow 0$ , as  $t \rightarrow \infty$ .

#### 4.2 Optimization strategies

The optimal PID controller gains are computed using GA, PSO and DE optimization techniques, the goal being to minimize the objective function  $J$  [Eq. (17)] and simultaneously remove the drawbacks and rigorous tuning routine associated with manual PID tuning. Each technique is a stochastic global search, zero-order method, therefore they do not require any derivatives to find the minimum [35,50]. All search spaces were bounded and realistic initial conditions were specified. The bounds and optimization parameters must be chosen such that the solution does not get caught in a local minimum and premature convergence problems do not arise.

The control structure for this algorithm shown in Fig. 5 is essentially the same as that for the manually tuned (non-optimal) PID-controlled AVSS, except that the objective function  $J$  [Eq. (17)] is computed within the loop and fed to the optimization routine which subsequently computes the PID gains for both the inner and outer control loops, respectively. Hence the total number of problem variables used for the quarter-car AVSS is six namely:  $K_P$ ,  $K_I$ ,  $K_D$ ,  $k_p$ ,  $k_i$ , and  $k_d$ . The optimization is performed offline using GA, PSO, and DE algorithms, respectively.

DE, GA, and PSO are random search optimization methods where the optimal solution is produced through the evolution of a random population set  $S = x_1, \dots, x_N$  with each individual denoted as  $x_i$ . These algorithms differ in the manner in which the population changes through each generation. The search space may be predefined to operate within a feasible region in order to improve computation time and convergence characteristics. Such a search space is chosen through intuitive reasoning and experience gained through manual tuning as in the case of PID controller tuning.

##### 4.2.1 Genetic algorithm (GA)

GA is a direct search algorithm that has attracted a lot of interest in recent years. It is a global optimization technique based on natural selection and the genetic reproduction concept. GA maintains a set  $S$  of candidate solutions. Traditionally, these candidate solutions (chromosomes) in GA are represented by binary-coded strings, but recently real coding of the strings has been preferred for continuous optimization problems. A real-coded GA treats chromosomes as points of real-valued numbers and it adapts the genetic operators of the binary coded GA accordingly. At each generation of GA, the old set  $S$  is updated by new offsprings obtained through the reproduction (crossover and mutation) process. The GA for minimization follows the four steps:

##### Algorithm 1 : The genetic algorithm

- **Step 1: Initialize.**
  - Generate  $N$  uniformly distributed random points from the search region  $\Omega$  and store the points and their corresponding function values in  $S = (x_1, \dots, x_N)$ .
  - Set generation counter  $k = 0$ . The initial condition  $x_0$  which in controller tuning corresponds

to the set of controller gains obtained through manual tuning.

– **Step 2: Stopping rule.**

If the stopping condition (e.g. the maximum value,  $k_{max}$ , of  $k$  has been reached) is achieved, then stop; otherwise continue to the next step.

– **Step 3: Generate offsprings.**

- Selection: select  $m \leq N$  points from  $S$  as parents, normally biased towards the better points.
- Crossover: pair the parents and create  $m$  new points (offsprings).
- Mutation: mutate an element (gene) of each offspring with probability  $p_v$ . Mutation is repeated if the mutated element is infeasible.

– **Step 4: Update  $S$ .**

- Replace the least fittest  $m$  points in  $S$  with the  $m$  offsprings.
- Set  $k = k + 1$  and go to Step 2.

In real-coded GA, for example, a crossover can be defined as follows: if  $x = (x_1, x_2, \dots, x_n)$  and  $y = (y_1, y_2, \dots, y_n)$  denote two parents and  $\tilde{x} = (\tilde{x}_1, \tilde{x}_2, \dots, \tilde{x}_n)$  and  $\tilde{y} = (\tilde{y}_1, \tilde{y}_2, \dots, \tilde{y}_n)$  denote the offsprings, then the offsprings are represented by:

$$\tilde{x}_i = \alpha_i x_i + (1 - \alpha_i) y_i \quad (22)$$

$$\tilde{y}_i = \alpha_i y_i + (1 - \alpha_i) x_i, \quad (23)$$

where  $\alpha_i$  are uniform random numbers, say in  $[-0.5, 1.5]$ . We have used  $N=500$ ,  $k_{max} = 150$  and  $m=250$ . Our numerical experiments suggest that the GA performs better with  $p_v = 0$ , taking some small probability for continuous variables.

#### 4.2.2 Particle swarm optimization (PSO)

PSO maintains a group of particles. At each iteration  $k$ , the  $i$ th particle is represented by a vector  $x_i^k$  in multidimensional space to characterize its position. The vector  $v_i^k$  is used to characterize its velocity. Thus, PSO maintains a set of positions

$$S = \{x_1^k, \dots, x_N^k\}$$

and a set of corresponding velocities

$$V = \{v_1^k, \dots, v_N^k\}.$$

Initially, the iteration counter  $k = 0$ , and the positions  $x_i^0$  and their corresponding velocities  $v_i^0$  are generated randomly from the search space  $\Omega$ . Each particle changes its position  $x_i^k$ , per iteration. The new position  $x_i^{k+1}$  of the  $i$ th particle ( $i = 1, 2, \dots, N$ ) is biased towards its best position  $p_i^k$  with best function value, referred to as personal best or *pbest*, found by the particle so far, and the very best position  $p_g^k$ , referred to as the global best or *gbest*, found by its companions. The *gbest* is the best position in the set

$$P = \{p_1^k, p_2^k, \dots, p_N^k\},$$

where  $p_i^0 = x_i^0, \forall i$ .

We regard a particle in  $S$  as good or bad depending on its personal best being a good or bad point in  $P$ . Consequently, we call the  $i$ th particle ( $j$ th particle) in  $S$  the worst (the best) if  $p_i^k$  ( $p_j^k$ ) is the least (best) fitted, with respect to function value, in  $P$ . We denote the best particle in  $S$  as  $p_g^k$ .

At each iteration  $k$ , the position  $x_i^k$  of the  $i$ th particle is updated by a velocity  $v_i^{k+1}$  which depends on three components: its current velocity  $v_i^k$  and the weighted difference vectors ( $p_i^k - x_i^k$ ) and ( $p_g^k - x_i^k$ ). Specifically, the set  $S$  is updated for the next iteration using

$$x_i^{k+1} = x_i^k + v_i^{k+1}, \quad (24)$$

where  $v_i^{k+1}$  is given as:

$$v_i^{k+1} = \omega v_i^k + r_1 c_1 (p_i^k - x_i^k) + r_2 c_2 (p_g^k - x_i^k). \quad (25)$$

The parameters  $r_1$  and  $r_2$  are uniformly distributed random numbers in  $[0, 1]$  and  $c_1$  and  $c_2$ , known as the cognitive and social parameters, respectively, are popularly chosen to be  $c_1 = c_2 = 2$ . Thus the values  $r_1 c_1$  and  $r_2 c_2$  introduce some stochastic weighting in the difference vectors ( $p_i^k - x_i^k$ ) and ( $p_g^k - x_i^k$ ), respectively. The set  $P$  is updated, as the new positions  $x_i^{k+1}$  are created, using the following rule

$$p_i^{k+1} = \begin{cases} x_i^{k+1} & \text{if } f(x_i^{k+1}) < f(p_i^k) \\ p_i^k & \text{otherwise.} \end{cases} \quad (26)$$

This process of updating the velocities  $v_i^k$ , positions  $x_i^k$ , *pbest*  $p_i^k$  and the *gbest*  $p_g^k$  is repeated until a user-defined stopping condition is met. This standard version of PSO is referred to as PSO-S, and its pseudo-code is presented below.

**Algorithm 2: The PSO algorithm [51]**

**Step 1: Initialization.**

- Step 1a: Initialize iteration counter  $k = 0$
- Step 1b: Initialize  $N$  random positions of the particles  $(x_i^k, i = 1, 2, \dots, N)$  and store them in  $S$ .
- Step 1c: Initialize  $N$  random velocities  $(v_i^k, i = 1, 2, \dots, N)$  and store them in  $V$ .
- Step 1d: Initialize  $N$   $pbest$   $(p_i^k, i = 1, 2, \dots, N)$  and store them in  $P$ .
- Step 1e: Set  $p_g^k$  equal the best  $pbest$  in  $P$ .

**Step 2: While not stopping criterion do**

- Step 2a: For each  $i$ th particle:
  - Update  $V$ :** Calculate  $v_i^{k+1}$  using (25)
  - Update  $S$ :** Calculate position  $x_i^{k+1}$  using (24)
  - Update  $P$ :** Update  $P$  using (26).
- Step 2b: Update  $gbest$   $p_g^k$ :

$$p_g^{k+1} = \arg \min_{i \in \{1, 2, \dots, N\}} f(p_i^{k+1}).$$

- Step 2c:  $k = k + 1$ .

We have used  $\omega=0.5$ ,  $k_{max}=100$  and  $N=100$ .

**4.2.3 Differential evolution (DE) optimization**

DE attempts to replace each point in  $S$  with a new better point. Therefore, in each iteration,  $N$  competitions are held to determine the members of  $S$  for the next iteration. The  $i$ -th ( $i = 1, \dots, N$ ) competition is held to replace  $x_i$  in  $S$ . Considering  $x_i$  as the target point a trial point,  $y_i$  is found from two points (parents), the point  $x_i$ , i.e. the target point and the point  $\hat{x}_i$  determined by the mutation operation. In its mutation phase DE randomly selects three distinct points  $x_{p(1)}, x_{p(2)}$  and  $x_{p(3)}$  from the current set  $S$ . None of these points should coincide with the current target point  $x_i$ . The weighted difference of any two points is then added to the third point which can be described as:

$$\hat{x}_i = x_{p(1)} + F(x_{p(2)} - x_{p(3)}) \tag{27}$$

where  $F > 0$  is a scaling factor, and  $x_{p(1)}$  is known as the base vector. If the point  $\hat{x}_i \notin \Omega$  then the mutation operation is repeated. The trial point  $y_i$  is found from its parents  $x_i$  and  $\hat{x}_i$  using the following crossover rule:

$$y_i^j = \begin{cases} \hat{x}_i^j & \text{if } R^j \leq C_R \text{ or } j = I_i \\ x_i^j & \text{if } R^j > C_R \text{ and } j \neq I_i, \end{cases} \tag{28}$$

where  $I_i$  is a randomly chosen integer in the set  $I$ , i.e.  $I_i \in I = \{1, 2, \dots, n\}$ ; the superscript  $j$  represents the  $j$ -th component of respective vectors;  $R^j \in (0, 1)$ , drawn uniformly for each  $j$ . The ultimate aim of the crossover rule (28) is to obtain the trial vector  $y_i$  with components coming from the components of target vector  $x_i$  and mutated vector  $\hat{x}_i$ . And this is ensured by introducing  $C_R$  and the set  $I$ . Notice that for  $C_R = 1$  the trial vector  $y_i$  is the replica of the mutated vector  $\hat{x}_i$ . The effect of  $C_R$  has been studied in [43,52] and it was found that  $C_R = 0.5$  is a good choice. The targeting process continues until all members of  $S$  are considered. After all  $N$  trial points  $y_i$  have been generated, acceptance is applied. In the acceptance phase the function value at the trial point,  $f(y_i)$ , is compared to  $f(x_i)$ , the value at the target point. If  $f(y_i) < f(x_i)$  then  $y_i$  replaces  $x_i$  in  $S$ , otherwise,  $S$  retains the original  $x_i$ . Reproduction (mutation and crossover) and acceptance continues until some stopping conditions are met [43].

**Algorithm 3: The DE Algorithm**

**Step 1: Determine the initial set**

$$S = \{x_1, \dots, x_N\}$$

where the points  $x_i, i = 1, \dots, N$  are sampled randomly in  $\Omega$ ; evaluate  $f(x)$  at each  $x_i, i = 1, \dots, N$ . Set iteration counter  $k = 0$ .

**Step 2: Stopping condition.**

If the stopping condition such as  $k > k_{max}$  is satisfied, select the fittest individual in  $S$  as the optimal solution and then stop; otherwise continue to the next step.

**Step 3: Generate points to replace points in  $S$  for the next population (or iteration).** For each  $x_i \in S$  ( $i = 1, \dots, N$ ), determine  $y_i$  by the following two operations:

**Mutation:**

$$\hat{x}_i = x_{p(1)} + F(x_{p(2)} - x_{p(3)})$$

where  $x_{p(1)}, x_{p(2)}$  and  $x_{p(3)}$  are three random vectors from  $S$  and  $F$  is a scaling factor. chosen randomly. The tournament selection is applied for each  $i$ . If the  $j$ -th component  $\hat{x}_i^j \notin \Omega$  then it is generated randomly.

**Table 2** PID controllers gains tuned using manual and evolutionary algorithms

Technique	Outer PID loop gains			Inner PID loop gains		
	$K_P$	$K_I$	$K_D$	$k_p$	$k_i$	$k_d$
Manual	17,000	0	1,400	0.002	0.004	0
GA	23,681	10	1,597	0.00193	0.0038	$6.448 \times 10^{-10}$
PSO	23,518	-15	2,507	0.00134	0.0023	0
DE	23,005	20	1,681	0.00195	0.0056	$6.386 \times 10^{-10}$

**Crossover** : Calculate the trial vector  $y_i$  corresponding to the target  $x_i$  from  $x_i$  and  $\hat{x}_i$  using the crossover rule (28).

#### Step 4: Acceptance rule to replace points in $S$ .

Select each trial vector  $y_i$  for the  $k + 1$  iteration using the acceptance criterion: replace  $x_i \in S$  with  $y_i$  if  $f(y_i) < f(x_i)$  otherwise retain  $x_i$ . Set  $k := k + 1$  and go to Step 2.

We have used  $C_R = 0.5$ ,  $F = 0.75$ ,  $k_{max} = 500$  and  $N = 100$ .

In relation to the structure of the DE, it is worth commenting on its potential to solve the problem from a computational point of view. Firstly, this algorithm has the ability to search the solution space more efficiently than most optimization algorithms. This is because the mutated individual  $\hat{x}_i$  for each individual  $x_i$  is determined based on only 3 randomly selected mutually independent individuals  $x_{p(1)}$ ,  $x_{p(2)}$ , and  $x_{p(3)}$  from the solution space  $S$ . Such a setup creates an excellent flexibility that permits candidate individuals to form anywhere in the solution space. Hence, many portions of the solutions space are expected to be explored with this configuration.

The second quality of the DE that makes it stand out with respect to other optimization algorithms is the fact that the  $x_i$  individual is replaced only if its respective candidate solution  $y_i$  has a better fitness value. This condition basically only allows progression or evolution of the individual if its fitness improves. Such a rule guarantees that the algorithm will converge to a solution. However, this condition tends to slow down convergence speed.

## 5 Results and discussion

A two-loop PID control system was utilized to effectively control the quarter-car AVSS. The actuator force

was generated by an electrohydraulic actuator which was stimulated by a control voltage in the range of  $\pm 10$  Volts. Numerical simulation of the designed AVSS was carried out in the *Matlab@/Simulink* environment. The AVSS was subjected to a deterministic road disturbance, which had the form of a sinusoidal road bump with a height of 0.11 m and a half-wavelength of 5 m. The vehicle travelled at 40 km/h.

The PID controllers were tuned using four different methods: manual, and EA-based optimization methods (DE, GA and PSO). The results obtained based on these methods were compared with those of the PVSS. The optimal gains obtained at the end of each iteration are listed in Table 2.

Figures 6 and 7 show the variation of the PID gains in the inner and outer feedback loops as the iteration progressed. The figures also show that optimal gains were already attained by the 100th iteration even though GA and DE were operated for 150 generations and iterations.

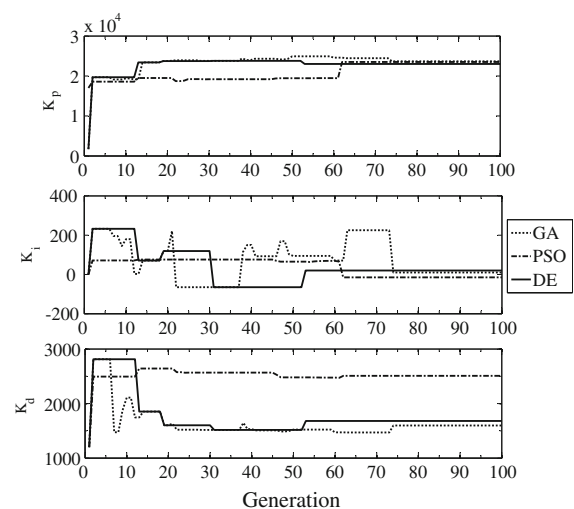


**Fig. 6** Variation of the outer PID feedback loop gains with iteration

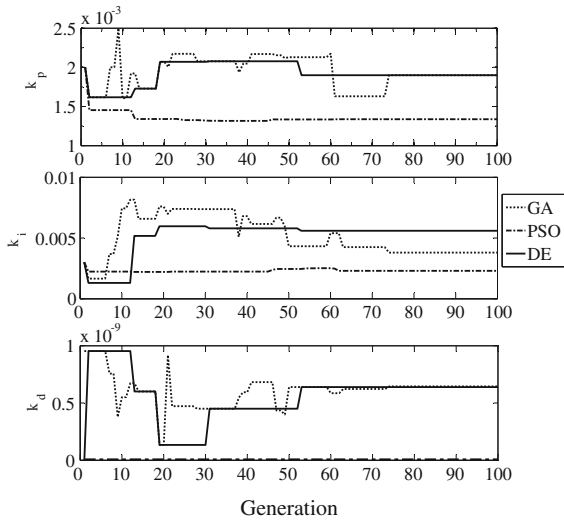


**Fig. 7** Variation of the inner PID feedback loop gains with iteration

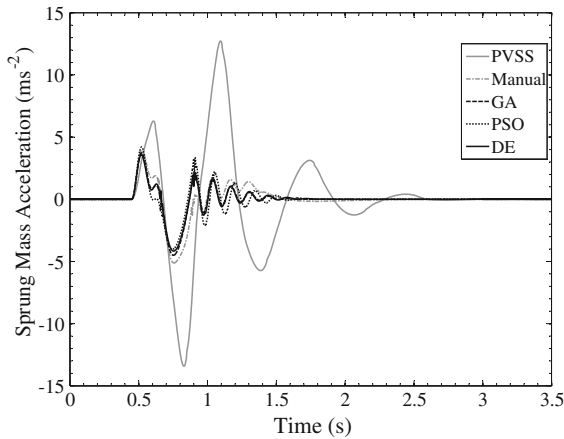


**Fig. 8** Heave acceleration time history

The vehicle body acceleration results are presented in Fig. 8. The improvement in the force transmitted to the vehicle body is evident in the AVSS with EA optimization. The peak body-heave acceleration for the PVSS is  $13.35 \text{ ms}^{-2}$ , DE-optimized case gave the best result of  $4.1 \text{ ms}^{-2}$ . This amounts to about 69% reduction in the force transmitted to the vehicle body on account of the road disturbance input.

In Fig. 9, multiple oscillations of the suspension system was cut down by the EA-optimized AVSS, such that settling time is reduced by about 36%, when compared with the PVSS. The least suspension travel peak value was attained by PSO-optimized AVSS controller. Other suspension performance objectives were traded-off for

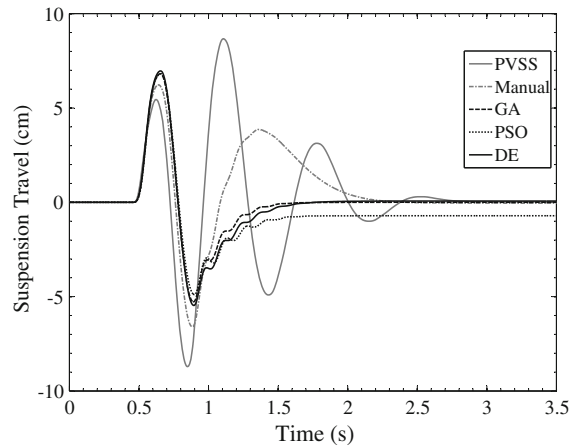


**Fig. 9** Suspension travel time history

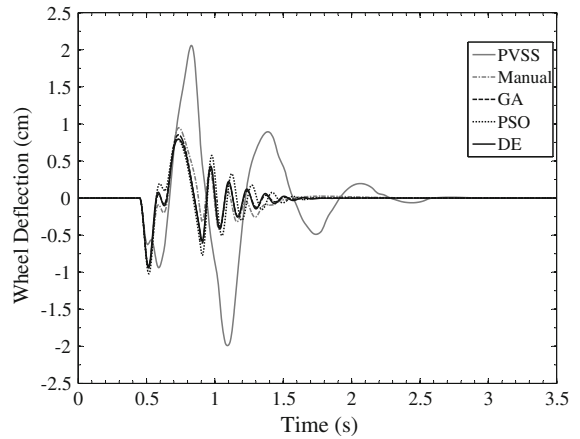


**Fig. 10** Wheel deflection time history

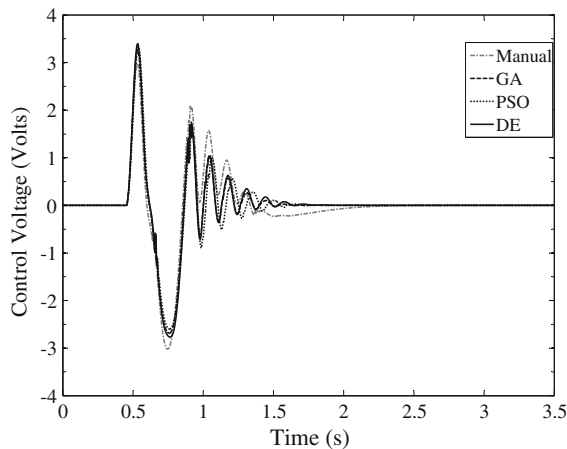
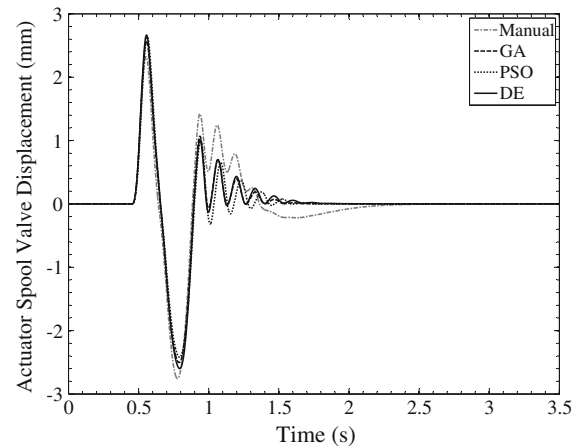
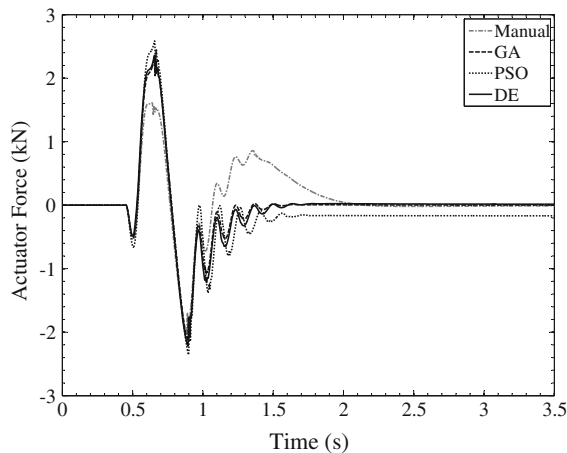
better suspension travel performance in the manually tuned controller.

The results for the wheel deflection is presented in Fig. 10. The trend is similar to those in the body-heave acceleration and suspension travel. The GA-optimized case has the best road-holding performance. Summary of the suspension performance based on the peak and RMS values are presented in Table 3.

The power consumption requirement for all the controllers were within allowable range as shown by Fig. 11 where the control voltages were within  $\pm 10$  Volts. Figure 12 presents the actuator force time history for the different controllers. While the lowest peak value of actuator force was generated by manually tuned AVSS controller, the PSO-optimized case had the largest actuator force peak value. In addition, the PSO-based case has a steady-state error of about  $0.2 \text{ kN}$ .

**Table 3** Summary of the vehicle suspension performance

		Passive	Manual	GA	DE	PSO
Suspension	RMS	2.50	2.30	1.90	1.80	1.70
Travel (cm)	Peak	8.70	6.40	6.90	7.10	6.80
Heave	RMS	4.10	1.62	0.98	0.94	0.96
Acceleration ( $\text{ms}^{-2}$ )	Peak	13.35	5.30	4.40	4.10	4.20
Wheel	RMS	0.64	0.24	0.21	0.23	0.22
Deflection (cm)	Peak	2.06	1.01	0.89	0.90	0.93
Settling time (s)		2.80	2.50	1.90	1.80	1.80

**Fig. 11** Control voltage time history**Fig. 13** Actuator spool-valve displacement time history**Fig. 12** Actuator force time history

The trend for the actuator spool-valve displacement in Fig. 13 is similar to that of the suspension travel (see Fig. 9) where the PSO-optimized case performance was marginally superior. Summary of these results are presented in Table 4.

Figures 14 and 15 show that the control system is stable in the bounded-input bounded-output (BIBO) sense as the system clearly settled with a steady-state error in the order of magnitude of 0.0001 m. Robustness analysis of the designed controller to parameter variations in the vehicle mass, tyre stiffness and speed was conducted for the DE-optimized case because it performed best. These specific parameters were chosen because the variations do occur in reality; as number of passengers and fuel do change over time; tyres do lose pressure during driving; and the vehicle speed does change. As the performed the best, this robustness analysis will be conducted for it. Parameter variations plots relating to suspension travel are presented in Figs. 14 and 15.

The steady-state error increased for both 20% increase and decrease in vehicle speed. An increase in vehicle speed produced weaker transient behaviour with an additional peak. The order of magnitude of the steady-state error for this parameter uncertainty is comparatively high but is acceptable considering the large

**Table 4** Summary of the vehicle suspension power consumption performance parameters

		Manual	GA	DE	PSO
Control voltage (Volts)	RMS	0.784	0.764	0.800	0.757
	Peak	2.90	3.30	3.40	3.20
Actuator force ( $kN$ )	RMS	0.550	0.593	0.631	0.659
	Peak	1.996	2.289	2.369	2.509
Actuator spool- Valve Displacement (m)	RMS	$5.503 \times 10^{-4}$	$5.086 \times 10^{-4}$	$5.277 \times 10^{-4}$	$5.054 \times 10^{-4}$
	Peak	0.0028	0.0026	0.0027	0.0026

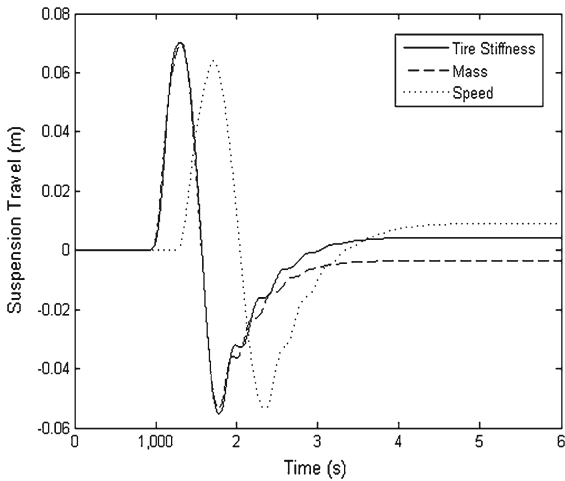


**Fig. 14** Suspension travel response of DE-based PID-controlled quarter-car system for  $-20\%$  variation in some selected parameters

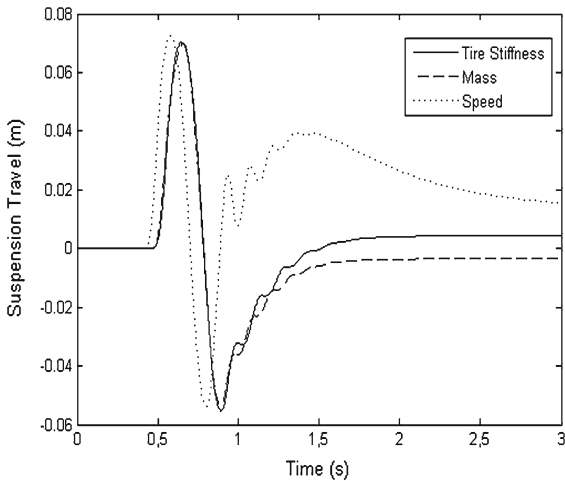


**Fig. 15** Suspension travel response of DE-based PID-controlled quarter-car system for  $+20\%$  variation in some selected parameters

degree of nonlinearities as well as the adverse effects of actuator dynamics. Variation in vehicle mass up to 20% did produce a steady-state error but it was 7% of the peak value and this makes it fairly acceptable. The same may be concluded for the case of a 20% variation in tyre stiffness as the largest steady-state error was only 12% of the peak value. Moreover, the system remained BIBO stable for all cases and this infers that the system is stable and has an acceptable degree of sensitivity to parameter variations.

The whole body vibration (WBV) frequency range of 0.5–80 Hz covers the critical frequency range for the humans (i.e. the vehicle resonance frequencies that needs to be avoided). Ride comfort is quantified on the basis of the RMS frequency-weighted vehicle body acceleration in the vertical direction, which prompts the use of the ISO 2631 weighting filter  $W_k$ . The human body is less sensitive to high-frequency vibrations, but ride discomfort is perceived at lower range (1–8 Hz) [47,49].

ISO 2631 provides guidelines and vibration sensitivity weighting specifications. Additional WBV specifications are provided in the European Commission Directive 2002/44/EC [48,49,53]. Figure 16 presents a pseudo-frequency domain analysis carried out using the power spectral density (PSD) estimates based on Welch algorithm in the *MATLAB*<sup>®</sup>/*Simulink* signal processing toolbox.

The following parameters are used in computing the Welch’s periodograms: the windowing function—Hanning window function; the number of points used in forming each fast Fourier transform,  $NFFT = 1,024$ ; length of the window,  $NWind = 256$ ; and the sampling frequency of the windows was set at 80 Hz to accommodate the WBV range.

A distinct resonance occurred at about 40 Hz for all the suspension systems, the vibration mode associ-

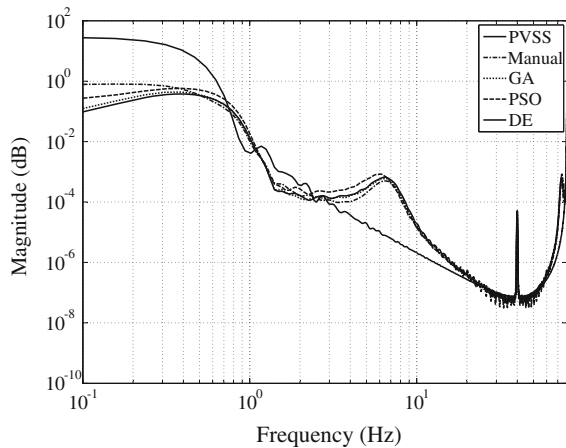


**Fig. 16** Frequency weighted RMS heave acceleration

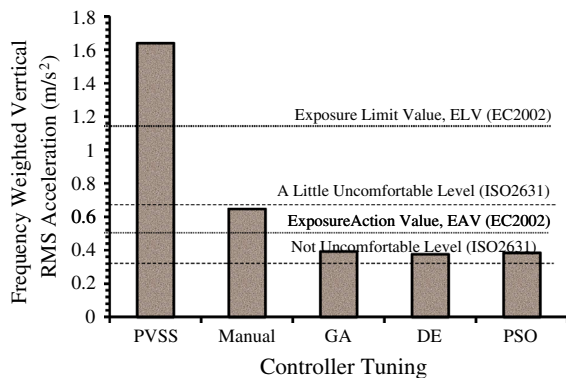


**Fig. 17** Ride comfort assessment

ated with this frequency could not be readily identified but the amplitude is  $<10^{-4}$  dB which is quite low. The AVSS had other minor resonance peaks but their magnitudes were also lower than 1 dB. All the other signals were attenuated except for the plot for passive suspension wherein signal magnitude was amplified within 0.1–0.8 Hz frequency range.

The frequency-weighted RMS value for the PVSS body-heave acceleration exceeded the exposure limit level (ELV) as stipulated by the European Commission Directive 2002/44/EC (see Fig. 17). However, this value for the manually tuned case exceeded the exposure action level (EAV) as stipulated by the same directive, but lies within the *a little uncomfortable* range stipulated by ISO 2631 [47–49].

The EA-optimized case had better ride comfort performance. Their performances were all below the EAV level and they were all within the *a little uncomfortable* range [47–49].

## 6 Conclusion

The performance of all the EA-optimized cases surpassed those of the manually tuned and the PVSS cases; especially in the vehicle body acceleration which was minimized to a third of the peak value for the PVSS. DE-optimized controller had the best overall performance. Although the PSO-optimized case results were close to those of the DE-optimized case, it exhibited steady-state errors in the suspension travel and the actuator force signal. This explains why it is less prominent than GA-optimized case with regard to engineering applications.

Optimal design of PID control is an effective tool in meeting hard design specifications such as those placed on ride comfort. They improved the steady-state characteristics of the suspension travel, and road holding as well as their transient behaviours. They tend to produce large derivative gains whose inherent ability to increase rise time tends to add chattering to the more sensitive outputs of the system. DE is the best optimal routine which exhibits a satisfactory robustness to system parameters variations. In terms of frequency response, each case was able to attenuate signals from 5 to 80 Hz. In the lower frequencies (0.01–5 Hz) the exposure levels were the worst. However, the AVSS cases did produce a significant improvement in this domain with RMS ride comfort values falling within the “Less Discomfort” range of the ISO 2631 (2003).

## References

- Pedro, J.O., Dahunsi, O.A.: Neural network based feedback linearization control of a servo-hydraulic vehicle suspension system. *Int. J. Appl. Math. Comput. Sci. AMCS* **21**(1), 137–147 (2011)
- Hrovat, D.: Survey of advanced suspension developments and related optimal control applications. *Automatica* **33**(10), 1781–1817 (1997)
- Fateh, M.M., Zirkohi, M.M.: Adaptive impedance control of a hydraulic suspension system using particle swarm optimisation. *Veh. Syst. Dyn.* **49**(12), 1951–1965 (2011)
- Yagiz, N., Sakman, L.E.: Robust sliding mode control of a full vehicle without suspension gap loss. *J. Vib. Control* **11**(11), 1357–1374 (2005)
- Cao, D., Song, X., Ahmadian, M.: Editor’s perspectives: road vehicle suspension design, dynamics and control. *Veh. Syst. Dyn.* **49**(1–2), 3–28 (2011)
- Cao, J., Liu, H., Li, P., Brown, D.: State of the art in vehicle active suspension adaptive control systems based on intelligent methodologies. *IEEE Trans. Intell. Transp. Syst.* **9**(3), 392–405 (2008)

7. Xue, X.D., Cheng, K.W.E., Zhang, Z., Lin, J.K., Wang, D.H., Bao, Y.J., Wong, M.K., Cheung, N.: Study of art of automotive active suspensions. In: proceedings of the 4th international conference on power electronics systems and applications (PESA), pp. 1–6. Hong Kong, China (2011)
8. He, Y., McPhee, J.: Application of optimisation algorithms and multibody dynamics to ground vehicle suspension design. *Int. J. Heavy Veh. Syst.* **14**(2), 158–192 (2007)
9. Wang, J., Xu, W., Chen, W.: Optimal hankel-norm reduction of active suspension model with application in suspension multiobjective control. *Int. J. Veh. Des.* **40**(1–3), 175–195 (2006)
10. Du, H., Zhang, N.:  $h_\infty$  control of active vehicle suspensions with actuator time delay. *J. Sound Vib.* **301**(1–2), 236–252 (2007)
11. Hassanzadeh, I., Alizadeh, G., Shirjoposht, N.P., Hashemzadeh, F.: A new optimal nonlinear approach to half car active suspension control. *IACSIT Int J. Eng. Technol.* **2**(1), 78–84 (2010)
12. Jin, Y., Luo, X.: Stochastic optimal active control of a half-car nonlinear suspension under random road excitation. *Nonlinear Dyn.* **72**(1–2), 185–195 (2013)
13. Chantranuwathana, S., Peng, H.: Adaptive robust force control for vehicle active suspensions. *Int. J. Adapt. Control Signal Process.* **18**(2), 83–102 (2004)
14. Feng, J.Z., Li, J., Yu, F.: Ga-based pid and fuzzy logic control for active vehicle suspension system. *Int. J. Automot. Technol.* **4**(4), 181–191 (2003)
15. Du, H., Zhang, N.: Static output feedback control for electro-hydraulic active suspensions via t-s fuzzy model approach. *J. Dyn. Syst. Meas. Control Trans. ASME* **131**(5), 051004-1–051004-11 (2009)
16. Nusantoro, G.D., Priyandoko, G.: Pid state feedback controller of a quarter car active suspension system. *J. Basic Appl. Sci. Res.* **1**(11), 2304–2309 (2011)
17. Sun, W., Gao, H., Kaynak, O.: Adaptive backstepping control for active suspension systems with hard constraints. *IEEE/ASME Trans. Mechatron.* **18**(3), 1072–1079 (2013)
18. Huang, C.-J., Li, T.-H.S., Chen, C.-C.: Fuzzy feedback linearization control for mimo nonlinear system and its application to full-vehicle suspension system. *Circuits Syst. Signal Process.* **28**(6), 959–991 (2009)
19. Chien, T.L., Chen, C.C., Tsai, M.C., Chen, Y.C.: Almost disturbance decoupling and tracking control for multi-input multi-output non-linear uncertain systems: application to a half-car active suspension system. *Proc. Inst. Mech. Eng. Part I J. Syst. Control Eng.* **223**(2), 215–227 (2009)
20. Kaynak, O., Erbatur, K., Ertugrul, M.: The fusion of computationally intelligent methodologies and sliding-mode control—a survey. *IEEE Trans. Industr. Electron.* **48**(1), 4–21 (2001)
21. Huang, S.J., Lin, W.C.: A neural network based sliding mode controller for active vehicle suspension. *Proc. Inst. Mech. Eng. Part D J. Automob. Eng.* **211**(11), 1381–1397 (2002)
22. Koshkouei, A.J., Burnham, K.J.: Sliding mode controllers for active suspensions. Proceedings of the 17th world congress. In: proceedings of the international federation of automatic control (IFAC), pp. 3416–3421. Seoul, Korea (2008)
23. Goncalves, E.N., Palhares, R.M., Takahashi, R.H.C.: A novel approach for  $h_2/h_\infty$  robust pid synthesis for uncertain systems. *J. Process Control* **18**(1), 19–26 (2008)
24. Ang, K.H., Chong, G., Li, Y.: Pid control system analysis, design, and technology. *IEEE Trans. Control Syst. Technol.* **13**(4), 559–576 (2005)
25. O’Dwyer, A.: Handbook of PI and PID controller tuning rules. Imperial College Press, London (2006)
26. Ekoru, J., Pedro, J.O.: Proportional-integral-derivative control of nonlinear half-car electro-hydraulic suspension systems. *J. Zhejiang Univ. Sci. A Appl. Phys. Eng.* **14**(6), 401–416 (2013)
27. Dahunsi, O.A., Pedro, J.O., Nyandoro, O.T.: System identification and neural network based pid control of servo-hydraulic vehicle suspension systems. *Trans. S. Afr. Inst. Elec. Eng. SAIEE Afr. Res. J. ARJ* **101**(3), 93–105 (2010)
28. Kaddissi, C., Saad, M., Kenne, J.P.: Interlaced backstepping and integrator forwarding for nonlinear control of an electro-hydraulic active suspension. *J. Vib. Control* **15**(1), 101–131 (2009)
29. Cetin, S., Akkaya, A.V.: Simulation and hybrid fuzzy-pid control for positioning of a hydraulic system. *Nonlinear Dyn.* **61**(3), 465–476 (2010)
30. Demir, O., Keskin, I., Cetin, S.: Modeling and control of a nonlinear half-vehicle suspension system: a hybrid fuzzy logic approach. *Nonlinear Dyn.* **67**(3), 2139–2151 (2012)
31. Chiou, J.-S., Tsai, S.-H., Liu, M.-T.: A pso-based adaptive fuzzy pid-controllers. *Simul. Model. Pract. Theory* **26**(8), 49–59 (2012)
32. Mohan, B.M., Sinha, A.: Analytical structure and stability analysis of a fuzzy pid controller. *Appl. Soft Comput.* **8**(1), 749–758 (2008)
33. Wang, Y.H., Shih, M.C.: Design of a genetic-algorithm-based self-tuning sliding fuzzy controller for an active suspension system. *Proc. Inst. Mech. Eng. Part I J. Syst. Control Eng.* **225**(3), 367–383 (2011)
34. Montazeri-GH, M., Soleymani, M.: Genetic optimization of a fuzzy active suspension system based on human sensitivity to the transmitted vibrations. *Proc. Inst. Mech. Eng. Part D J. Automob. Eng.* **222**(10), 1769–1780 (2008)
35. Iruthayarajan, M.W., Baskar, S.: Evolutionary algorithms based design of multivariable pid controller. *Expert Syst. Appl.* **36**(5), 9159–9167 (2009)
36. Fleming, P.J., Purshouse, R.C.: Evolutionary algorithms in control systems engineering: a survey. *Control Eng. Pract.* **10**, 1223–1241 (2002)
37. Konak, A., Coit, D.W., Smith, A.E.: Multi-objective optimization using genetic algorithms: a tutorial. *Reliab. Eng. Syst. Saf.* **91**, 992–1007 (2006)
38. Alfi, A., Fateh, M.M.: Identification of nonlinear systems using modified particle swarm optimisation: a hydraulic suspension system. *Veh. Sys. Dyn.* **49**(6), 871–887 (2011)
39. Pedro, J., Dangor, M., Dahunsi, O.A., Ali, M.M.: (2013) Differential evolution-based PID control of nonlinear full-car electrohydraulic suspensions. *Math. Prob. Eng.* **2013**(261582), 1–13 (2013)
40. Shi, Y., Eberhart, R.C.: A modified particle swarm optimizer. In: proceedings of the IEEE international conference on evolutionary computation, pp. 69–73, Anchorage, Alaska, USA (1998)

41. Zhan, Z.H., Zhang, J., Li, Y., Chung, H.: Adaptive particle swarm optimization. *IEEE Trans. Syst. Man Cybern. Part B Cybern.* **39**(6), 1362–1381 (2009)
42. Wai, R.-J., Lee, J.-D., Chuang, K.-L.: Real-time pid control strategy for maglev transportation system via particle swarm optimization. *IEEE Trans. Industr. Electron.* **58**(2), 629–646 (2011)
43. Kaelo, P., Ali, M.M.: Differential evolution algorithms using hybrid mutation. *Comput. Optim. Appl.* **37**, 231–246 (2007)
44. Ali, M.M.: Differential evolution with generalized differentials. *J. Comput. Appl. Math.* **235**(8), 2205–2216 (2011)
45. Gaspar, P., Szaszi, I., Bokor, J.: Active suspension design using linear parameter varying control. *Int. J. Auton. Syst. IJVAS* **1**(2), 206–221 (2003)
46. Gysen, B.L.J., Paulides, J.J.H., Janssen, J.L.G., Lomonova, E.A.: Active electromagnetic suspension system for improved vehicle dynamics. *IEEE Trans. Veh. Technol.* **59**(3), 1156–1163 (2010)
47. Griffin, M.J.: Discomfort from feeling vehicle vibration. *Veh. Syst. Dyn.* **45**(7–8), 679–698 (2007)
48. European commission: Directive 2002/44/EC of the European parliament and the council of 25 June 2002 on the minimum health and safety requirements regarding the exposure of workers to the risk arising from physical agents (vibration). *Official Journal of the European Communities, Luxembourg* (2002)
49. ISO 2631: Mechanical vibration and shock—evaluation of human exposure to whole-body vibration—Part 1: General requirements. International organization for standardization, Geneva, Switzerland (2003)
50. Crews, J.H., Mattson, M.G., Buckner, G.D.: Multi-objective control optimization for semi-active vehicle suspensions. *J. Sound Vib.* **330**(23), 5502–5516 (2011)
51. Kennedy, J., Eberhart, R.C.: The particle swarm: social adaptation in information-processing systems. In: Corne, D., Dorigo, M., Glover, F. (eds.) *New Ideas in Optimization*, pp. 379–387. McGraw-Hill, Cambridge (1999)
52. Ali, M.M., Torn, A.: Population set-based global optimization algorithms: some modifications and numerical studies. *Comput. Optim. Appl.* **31**(10), 1703–1725 (2004)
53. Zuo, L., Nayfeh, S.A.: Low order continuous-time filters for approximation of the iso 2631–1 human vibration sensitivity weightings. *J. Sound Vib.* **265**(2), 459–465 (2003)